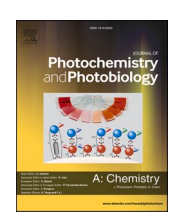
FISEVIER

Contents lists available at ScienceDirect

### Journal of Photochemistry & Photobiology, A: Chemistry

journal homepage: www.elsevier.com/locate/jphotochem





# Effect of polymer host matrix on multi-stage isomerization kinetics of DASA photochromes

Sara Sandlass<sup>a</sup>, Friedrich Stricker<sup>b,1</sup>, Daniel Fragoso<sup>a</sup>, Javier Read de Alaniz<sup>b</sup>, Michael J. Gordon<sup>a,\*</sup>

- <sup>a</sup> Department of Chemical Engineering, University of California Santa Barbara, Santa Barbara, CA 93106, USA
- <sup>b</sup> Department of Chemistry, University of California Santa Barbara, Santa Barbara, CA 93106, USA

#### ARTICLE INFO

Keywords:
Donor-acceptor Stenhouse Adducts
Visible spectroscopy
Kinetic modeling
Photoswitch
Polymers

#### ABSTRACT

Molecular photoswitches provide a means for imparting synthetic structures with intrinsically logical and highly tunable photoresponsive properties. One variety of organic photoswitches known as Donor-Acceptor Stenhouse Adducts, or DASAs, are promising candidates for next generation light responsive materials because of their unique ability to stabilize three photochemically distinct isomeric states in solution, while their counterparts are strictly limited to binary state behavior. In this work, we show how polymethacrylate host matrices shift the energetic landscape of DASA relative to solution, prohibiting accumulation of an intermediate third isomeric state by decelerating critical steps in the photoswitching mechanism. Specifically, we employ a dual-wavelength, phase locked detection scheme to probe thermal isomerizations in the switching process that occur at fast (~ms) time scales that are inaccessible by standard UV–Vis spectroscopic techniques. The results of this study provide valuable insight into the mechanism of multistate DASA reactivity and establish the foundation necessary to guide future efforts in offsetting kinetic matrix effects to enable dynamic, three state photoswitching in polymeric hosts

#### 1. Introduction

With applications from consumer products to medical devices, light-responsive "smart" materials are at the forefront of research and development endeavors worldwide. While the field encompasses a broad range of chemistries, these materials all rely on some form of molecular or atomic-scale logic to impart synthetic structures with optical stimuli-responsive properties. Despite the unmatched spaciotemporal tunability of light (e.g., wavelength, intensity, and polarization), most examples of photoresponsive smart materials employ binary logic, i.e., they convert to from state A to state B when the light is on and revert to A either when the light is removed (T-type) or when a secondary wavelength is introduced (P-type). Multistate (>2) photoresponsive materials have been demonstrated by combining absorbance-shifted binary switches [1–3], but the introduction of single species multistate photoswitches could enhance a device's capacity for complex logic and improve its dynamic reconfigurability.

Organic photoswitches are a class of small molecule building blocks

that are well suited for photo-responsive material applications because they undergo absorption-induced conformational changes, including E/Z isomerization and/or (de)cyclization, that can be leveraged into macroscopic structural responses. For example, researchers have demonstrated how changes in the polarization state of spiropyran upon photoisomerization can lead to macroscopic changes in hydrophilicity [4,5], ion permeability [6], surface tension [7,8], and adhesion [9]. Additionally, the axial contraction of azobenzene during trans to cis photoisomerization has been leveraged to generate large strains in aligned networks [10–13] and induce solid to liquid phase transitions in entangled polymers [14].

Donor-Acceptor Stenhouse Adducts (DASAs) are among a group of photoswitches, known as negative photochromes, that isomerize from a highly absorbing to a non-absorbing form upon photoexcitation, and thermally revert to their absorbing states in the dark (T-type) [15]. Aside from the large shift in absorptivity, DASA isomerization is accompanied by a change in molecular polarization and photothermal heating. These effects have enabled DASA-based photothermal bending actuation of

<sup>\*</sup> Corresponding author.

E-mail address: gordon@ucsb.edu (M.J. Gordon).

Present address: Department of Materials Science and Mechanical Engineering, Harvard University, Cambridge, MA 02138, USA.

polymer films [16,17], self-sustained convective flow [18], controlled (de)wetting at liquid—liquid interfaces [8], and light-controlled release of encapsulated cargo from polymer micelles [19]. Unlike azobenzene, which requires damaging UV light to undergo photoisomerization, light responsive materials leveraging DASA can be manipulated with visible light. While this is highly advantageous for biomedical applications, DASA photoswitching in aqueous environments has only been demonstrated when stabilized either in phase separated lipid lysosomes [20,21] or in polymer micelles [22] and vesicles [19]. In addition to facilitating photoswitching in water, DASA-polymer blends and conjugates based on a variety of elastomeric and amorphous thermoplastic polymers have enabled promising applications in light-powered soft robotics [16,17], soft chemo- and temperature sensing [23,24], and photopatterning of polymer films [2,25].

Despite their appearance as binary T-type switches, the isomerization of DASA from colored to colorless proceeds through an initial P/Ttype actinic step, followed by a series of thermal isomerizations, generating intermediates with distinct photo-reactivity from the ground state isomer in the process [26–28]. This behavior has shown to enable dynamic dual wavelength control over the distribution of three isomeric states of DASA in solution, a rare example of a single molecule ternary photochrome [26,29]. A simplified model for the photobleaching of DASA from the colored, ground state linear isomer (A) to a set of colorless closed ring isomers (C) under irradiation at the primary absorption band of A is provided in Fig. 1. By preferentially addressing the metastable and spectroscopically indistinguishable intermediates B and **B'** with a second wavelength of light, the rate of **B** isomerization back to A can be enhanced relative to the rate of B' electrocyclization to generate C, a thermal step. Accelerated reversion of B to A effectively gates cyclization to C and extends the lifetime of the colored isomer, A, under constant, dual wavelength irradiation.

A major challenge in exploiting DASA's inherent multistate nature is the need for increasingly higher photon fluxes in systems where the thermal lifetimes of **B** and **B'** are too short for them to accumulate in sufficient concentrations. By sterically modifying the DASA architecture to tune the energetic landscape, Stricker et al. demonstrated how these intermediates can be stabilized by raising the B to A and B' to C activation barriers. Consequently, the loss of absorbance that occurred following the accumulation of C when irradiating A with green light was successfully gated by the simultaneous photoexcitation of B/B' with red light [26]. While this study only explored the effect of intramolecular steric effects, intermolecular interactions between DASA and its host environment have also been widely reported to shift the energetic landscape of photoswitching. For example, polarizing interactions between DASA and its environment, including dipole-dipole and hydrogen bonding, are expected to play a role in the kinetics and thermodynamics of photoswitching based on kinetic studies performed in a variety of polar solvents [30,31]. In addition, the study of DASA in polymer films has identified a link between the host matrix glass transition temperature and rates of photobleaching and thermal recovery, suggesting that viscous forces raise the energetic barriers for certain bond rotations necessary for isomerization [1,32]. However, little is known about how individual steps in the overall isomerization process respond to changes in the extramolecular environment, especially in polymers. This is because the time scales corresponding to thermal isomerizations through which **B** regenerates **A**, or proceeds to **B**' and **C**, have remained challenging to probe spectroscopically. Without these crucial mechanistic insights, it is challenging to predict whether the multistate photoreactivity demonstrated by Stricker et al. in solution is attainable in DASA-polymer blends. As a result, applications that rely on DASA photoswitching in polymers cannot leverage its unique multistate nature to expand their capabilities.

In this work, we show that the capacity for dual wavelength, multistate kinetic control of DASA is diminished in blends of poly(butyl methacrylate) (PBMA) and poly(methyl methacrylate) (PMMA) relative to a solution in toluene. To provide mechanistic insight into these results, we employ a dynamic, phase-locked optical measurement technique with greater temporal resolution and sensitivity than standard UV–Vis to probe the rapid formation and decay kinetics of the B/B' intermediates in these varied environments. While the pseudo-equilibrium intermediate population established under irradiation of A is reduced in polymer blends, specifically in glassy PMMA, we use

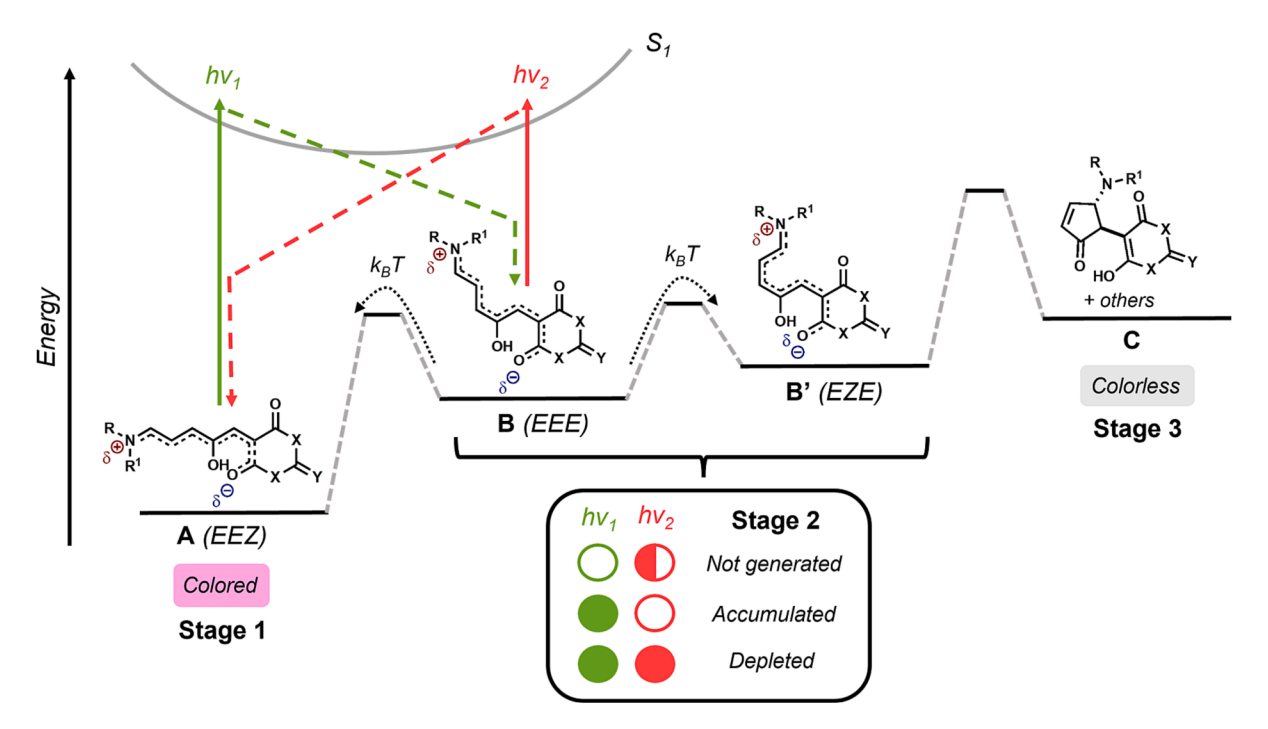


Fig. 1. Schematic representation of DASA photoswitching mechanism under dual wavelength control.  $Stage\ 2$  is generated under irradiation at wavelength 1 (hv<sub>1</sub>) and accumulates under single wavelength exposure (solid green). The addition of a second, red-shifted wavelength (hv<sub>2</sub>) depletes the molecular population of  $stage\ 2$  by introducing a photochemical pathway (dashed red) to regenerate  $stage\ 1$  (A). Depletion of  $stage\ 2$  results in slower colored to colorless photoswitching by slowing the rate of C production. Bond orientations (E vs. Z) within the conjugated system are included to distinguish relevant isomers.

kinetic modeling to show that the thermal stability of these intermediate isomers, once formed, has minimal dependence on the nature of the environment. Instead, the diminished capacity for multistate kinetic control in PBMA and PMMA can be attributed to matrix-induced effects that specifically impede the initial actinic conversion from A to B, limiting accumulation of the photochemically distinct intermediates that make DASA unique.

#### 2. Methods

#### 2.1. Sample preparation

The specific DASA molecule used in this study (Fig. 2B) was synthesized and isolated according to the method in Sroda et al. [30]. DASA-loaded polymer films were fabricated by casting a solution of DASA and either poly(butyl methacrylate) (PBMA, avg. 211 kDa) or poly (methyl methacrylate) (PMMA, avg. 120 kDa) in dichloromethane onto a glass supported polyethylene terephthalate (PET) substrate (50 µm thickness). The resulting bilayer films were peeled from their glass supports and dried in vacuum overnight. The films were cast and dried at room temperature, approximately 23 °C. Glass transition temperatures for the polymers were measured by DSC to be 33  $^{\circ}$ C and 98  $^{\circ}$ C for PBMA and PMMA, respectively. When blended with 1 wt% of DASA, the corresponding glass transition temperatures decreased to 32 °C and 82 °C. After drying, the spatially averaged thicknesses of the DASAloaded polymethacrylate layers were estimated to be approximately  $10\text{--}15~\mu\text{m}$ , based on the known substrate surface area, the masses of the deposited polymers, and their densities. Due to the relatively low precision of the drop casting method compared to alternative manufacturing methods (e.g., spin coating, drawing), the localized film thicknesses were subject to variability of up to several microns. We deemed this degree of imprecision acceptable because the analysis performed in this study did not require a robust measure of sample dimensions. PBMA and PMMA were purchased from Sigma Aldrich and the PET films were from McMaster Carr.

#### 2.2. Spectroscopic characterization

#### 2.2.1. Broadband UV-Vis pump probe spectroscopy

Broadband transmission measurements were performed on an Ocean Optics USB4000 UV–Vis Spectrometer from approximately 300 nm-800

nm using a fiber-coupled deuterium halogen broadband probe light (Mikropack DH-2000-BAL) and LabVIEW-controlled data acquisition. The A and B/B' isomers were optically pumped with a fiber-coupled 532 nm Nd:YAG laser (Q-BAIHE), outfitted with cleanup optics to remove residual infrared radiation, and a pair of 620 nm LEDs (Cree XLamp in color red-orange), respectively. The LEDs were angled and focused to intersect at the sample surface for maximum power, and the LED current loads were metered with a power supply. A solenoidpowered beam flag was used to control the 532 nm beam exposure time while the 620 nm LEDs were electrically gated. Both were driven through LabVIEW (National Instruments PCI-6220). Every 5 s, optical pumping was paused for approximately 70 ms before collecting transmission spectra. Signal integration was performed over the subsequent 30 ms before resuming irradiation. The initial 70 ms delay time was necessary to accommodate the mechanical delay of the 532 nm beam flag, preventing contamination of the transmission measurement with scattered pump light. Emission profiles for the photoexcitation sources are overlaid with the A and B/B' absorption profiles in Supplementary Figs. S.5, S.7, and S.9 for DASA in toluene, PBMA, and PMMA, respectively.

Film samples were cut to approximately 1 cm  $\times$  1 cm squares and adhered using double stick tape to a removable sample puck. The DASA-loaded layer was oriented facing normal to the incident probe beam. The pump beams were introduced off normal by  $10^\circ\text{--}45^\circ$ . Solution samples were prepared by pipetting 80  $\mu L$  into a 1 cm wide glass cuvette with a path length of 1 mm. This volume was used to ensure the entire sample resided in the pump source exposure area and minimized diffusion effects in the observed photoswitching rates.

#### 2.2.2. Frequency modulated pump probe spectroscopy (FMPPS)

To passively probe the kinetics of photochemically active species with enhanced temporal resolution and sensitivity than is possible by traditional UV–Vis absorption spectroscopy, we developed a wavelength-indiscriminate, phase locked detection scheme. This method, termed Frequency Modulated Pump Probe Spectroscopy (FMPPS, Fig. 2), utilized modulation of two narrow bandwidth, spectrally shifted probe lights to simultaneously track the absorbances of  $\bf A$  and  $\bf B/B'$ .

A 532 nm probe line was generated to track the absorbance of the A isomer by reflecting a fraction of the continuous wave 532 nm pump line (Section 2.2.1) with a glass slide, chopping the beam at 506 Hz, and

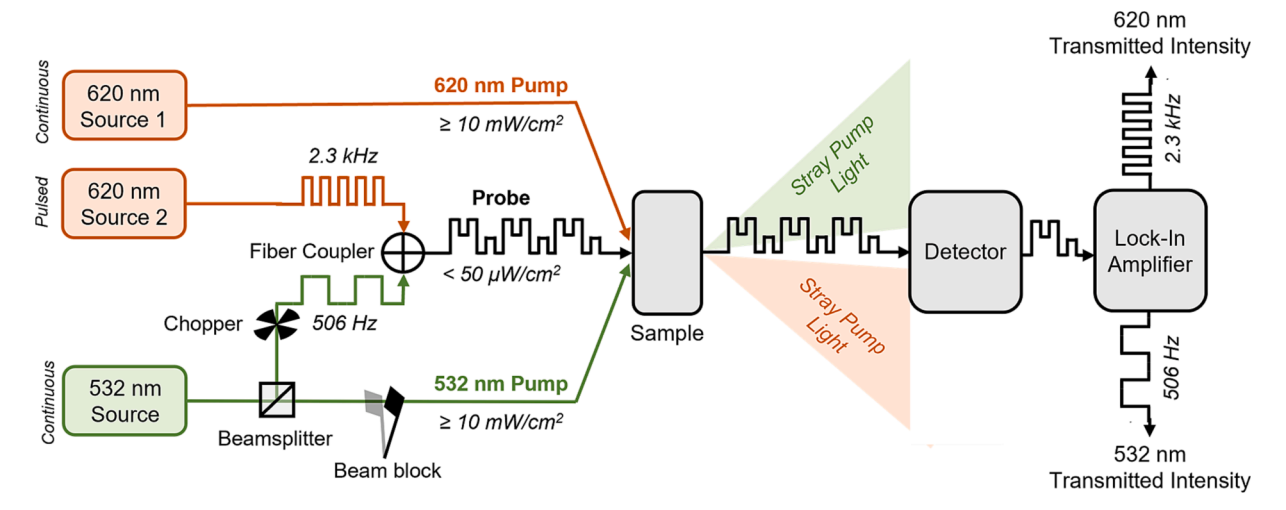


Fig. 2. Schematic illustration of the FMPPS technique. A 532 nm continuous wave laser and a 620 nm LED were used to optically pump the sample. A small portion of the 532 nm pump line was split off, chopped at 506 Hz, and fiber coupled together with a portion of the light emitted by a separate but spectrally identical 620 nm LED that was electrically gated with a 2.3 kHz square wave. The combined beam was passed through the sample and collected with a photodetector. Lock-in amplifiers were used to deconvolve the transmitted 532 nm and 620 nm probe beam intensities according to their modulation frequencies and isolate them from unmodulated background radiation from the pump beams.

reflecting the beam again off a second glass slide into an optical fiber. To monitor the combined absorbances of the B and B' isomers, a second 620 nm LED, spectrally identical to the pumping source described in Section 2.2.1, was electronically gated with a 2.3 kHz square wave (33120A 15 MHz Function Generator, Agilent Tech.), and coupled into the same fiber as the 532 nm probe. The composite beam was passed through the sample in an identical fashion as the broadband probe light in Section 2.2.1 but was collected with a Thorlabs PDA 36A Si Switchable Gain Photodetector instead of a spectrometer. The output signal from the detector was passed into a pair of Stanford Research SR830 Lock-In Amplifiers to deconvolve the two probe amplitudes according to their modulation frequencies. A schematic illustration of the technique is provided in Fig. 2. Negligible spectral overlap between the 532 nm and 620 nm probe beams with the absorbance profiles of B/B' and A, respectively, meant that further deconvolution to isolate the absorbance of each isomeric state was unnecessary.

Lock-in amplification provided a means for performing highly accurate transmission measurements with especially low intensity light. To ensure the samples were optically probed as passively as possible, the probe intensities were maintained below 50  $\mu\text{W/cm}^2$ . The lock-in time constants were selected to ensure accurate signal integration over at least 5 periods; 10 ms and 3 ms on the high and low frequency modulated sources, respectively. LabVIEW data acquisition (National Instruments PCI-6220) was used for real-time measurements at 25 Hz of the transmitted probe intensities during optical excitation and relaxation.

Optical excitation (pumping) occurred by the same approach as outlined in S.1.2.2 but without pausing to collect absorbance data. This was possible because the use of frequency selective detection ensured that unmodulated background radiation from the scattered pump beams did not contaminate the measurement. All samples were pumped with 532 nm light for 600 ms, followed by 3–8 s of pumping with different

intensities of 620 nm light. The pump timing was controlled by LabVIEW as was outlined in Section 2.2.1.

#### 3. Results and discussion

#### 3.1. Kinetic model of multistate photoswitching

Altered rates of DASA isomerization with the transition from solution to amorphous polymers have been reported previously [1,32,33] and were expected to result in different multistate reactivity from that observed in solution by Stricker and coworkers [26]. To quantify this effect, we performed a series of spectrokinetic measurements on a single, first generation DASA structure (Fig. 3B) blended in PBMA and PMMA. To benchmark these results against a representative solution-based system, we tested a third mixture of DASA in toluene.

Initially, we confirmed the presence of a spectroscopically distinguishable intermediate that was populated following irradiation of A in toluene, PBMA, and PMMA. After allowing sufficient time in the dark to deplete any transient intermediates, the only absorbing form of DASA assumed to be present was A, the thermodynamically favored isomer. This is validated by the existence of single absorbance peak at 547 nm in toluene, 540 nm in PBMA, and 535 nm in PMMA (Fig. S.2). The slight blue shift observed in PBMA and PMMA can likely be attributed to increasing environmental polarity and aligns with the result of Sroda et al. [30]. Irradiating A for 5 s resulted in the formation of a secondary peak, approximately 60 nm red-shifted from the initial  $\lambda_{max}$ . The position of this peak relative to A was roughly consistent in toluene (Fig. 3A), PBMA (Fig. S.6), and PMMA (Fig. S.8), and has been attributed to the metastable intermediates, **B** and **B**', in previous studies [26,34]. Significant spectral overlap between the B and B' intermediates meant they could not practically be spectroscopically distinguished in the visible wavelength regime.

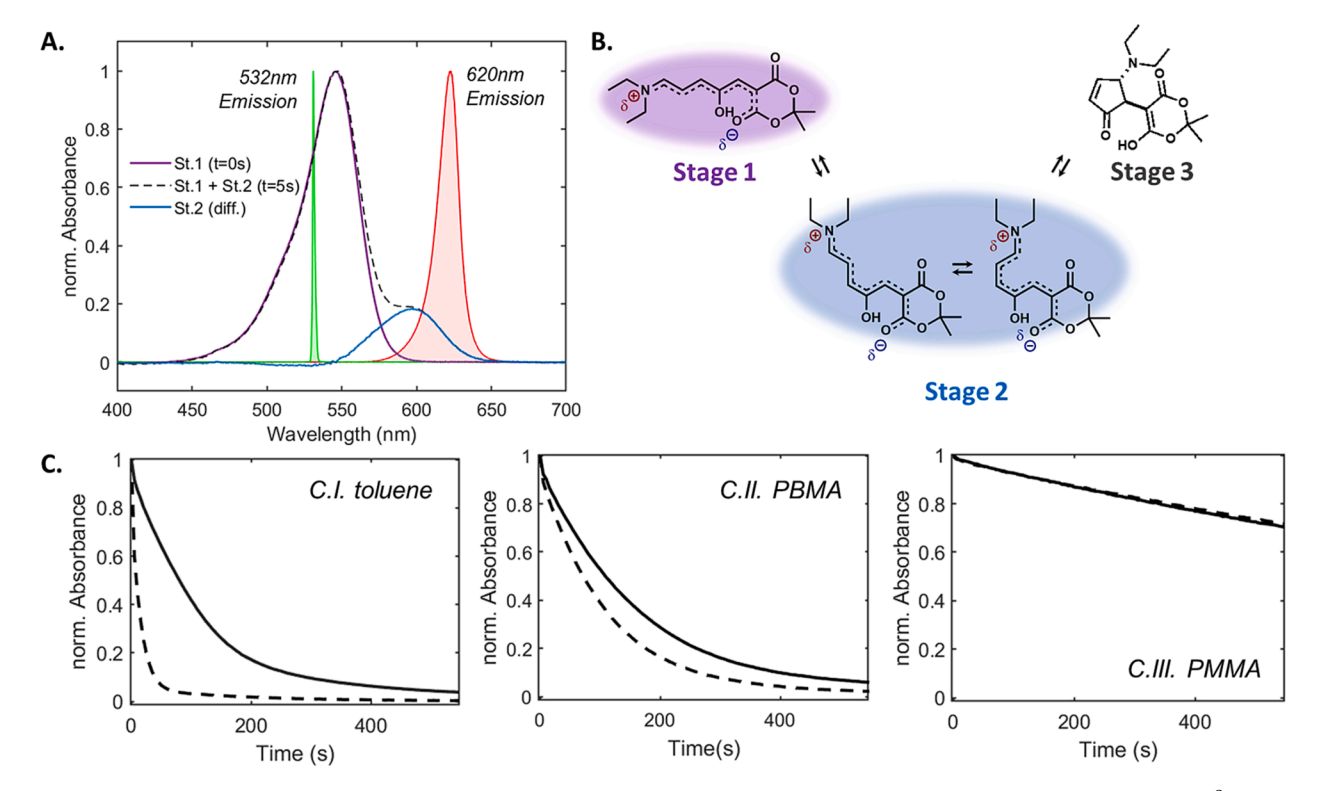


Fig. 3. (A) Overlaid normalized absorption spectra for DASA 1.0 in toluene at t=0 s (solid, violet) and after 5 s of optical pumping with 9.2 mW/cm<sup>2</sup> of 532 nm light (dashed black). The *stage 2* absorption profile (solid, dark blue) was computed from their difference. Emission profiles for light sources used in this study are shaded. See Supplementary Figs. S.5 and S.7 for absorption profiles in PBMA and PMMA. (B) Simplified photoswitching mechanism of DASA used in this study. (C) Photoswitching (as measured by absorbance at the  $\lambda_{max}$  of Fig. 2A) under 9.2 mW/cm<sup>2</sup> 532 nm with (solid) and without (dashed) 78 mW/cm<sup>2</sup> of 620 nm in (C.I) toluene (0.0179 mM), (C.II) PBMA (1 wt%), and (C.III) PMMA (1 wt%). Normalization constants are provided in Supplementary Table S.2.

With this in mind, we employed a reduced form of the four-state mechanistic model illustrated in Fig. 1, designed to account only for the three states that were photochemically distinct:  $stage\ 1$  (A),  $stage\ 2$  (B and B'), and  $stage\ 3$  (C).  $Stage\ 1$  was assumed to exclusively contain the linear form, triene isomer, A, and could be converted to  $stage\ 2$  by actinic E/Z isomerization.  $Stage\ 2$  contained both short-lived intermediates B and B' and could either thermally proceed through a  $4\pi$  electrocyclization to  $stage\ 3$  or decay back to  $stage\ 1$ . The reverse isomerization to regenerate  $stage\ 1$  could be accelerated by leveraging a parallel actinic pathway promoted under the irradiation of  $stage\ 2$ .  $Stage\ 3$  contained all non-absorbing, closed form isomers and could slowly reform  $stage\ 2$  in solution or persist as a kinetically trapped state in polymer blends. A schematic illustration of the simplified model is included in Fig. 1.

To ensure clarity while keeping consistent terminology with traditional 2-state DASA models, we differentiated between photoisomerization and photobleaching, where the former refers to the single step actinic interconversions of A and B, while the latter refers to the loss of absorbance (as measured by the absorbance of stage 1) with the net conversion of stage 1 to stage 3 under irradiation. By this convention, photobleaching could occur either by "single wavelength" exposure to address stage 1 in isolation or by "dual wavelength" exposure to simultaneously address stages 1 and 2. Addressing stage 2 during photobleaching allowed for photokinetic control in the bleaching rate by promoting the reformation of stage 1 from stage 2 and slowing the production of stage 3 as a result. Throughout this work, stages 1 and 2 were excited with a 532 nm laser and a 620 nm LED, respectively. Emission profiles for these light sources are overlaid with the absorbance profiles of each stage in Fig. 3.A and were selected among those commercially available to maximize absorptivity of the desired stage while minimizing overlap with the opposing stage.

#### 3.2. Dual wavelength multistate DASA control in polymer blends

To determine the degree of photokinetic control achievable in PBMA, PMMA, and toluene, we subjected DASA in each environment to two different bleaching conditions. The first of these exposure conditions was the single wavelength control to excite stage 1 alone (532 nm, 9.2 mW/cm<sup>2</sup>), while the second addressed stages 1 and 2 with dual wavelength irradiation (532 nm:  $9.2 \text{ mW/cm}^2$  and 620 nm:  $78 \text{ mW/cm}^2$ ). The samples were selected to ensure similar starting absorbances at the stage 1 excitation wavelength (Table S.2). This ensured their rates of photobleaching depended only on the intrinsic properties of DASA and not on the phase or dimensions of the host environment. For justification of this, refer to the kinetic model derived in Supplementary Eqs. S.3 and S.4. Based on the results of this study, presented in Fig. 3C, we determined that while addressing stage 2 with a secondary wavelength of light resulted in a marked deceleration in the rate of bleaching in toluene, polymer blends of DASA in PBMA and PMMA were less receptive to photokinetic control. In fact, DASA in PMMA displayed no discernable kinetic effect induced by photochemically addressing stage 2 during bleaching with the optical fluxes tested.

Isolating the cause of the diminished photokinetic control demonstrated in polymer blends requires a greater understanding of the *stage 2* formation kinetics in each host medium. To facilitate this exploration, we used the aforementioned FMPPS method to track the rapid interchange of isomers in *stages 1* and 2 that occurred to establish a dynamic equilibrium under irradiation of *stage 1*. The exposure times required to reach equilibrium, as indicated by the end of *stage 2* accumulation, were between 0.1 and 1 s, depending on the DASA host environment. The shortened time scale for this process as compared to the several minutes required for photobleaching necessitated a spectroscopic method with greater temporal resolution than traditional UV–Vis. For this reason, FMPPS was more suitable than traditional broadband UV–Vis absorption spectroscopy.

The results of this experiment are provided in Fig. 4 and, when compared with the results obtained under prolonged, dual-wavelength

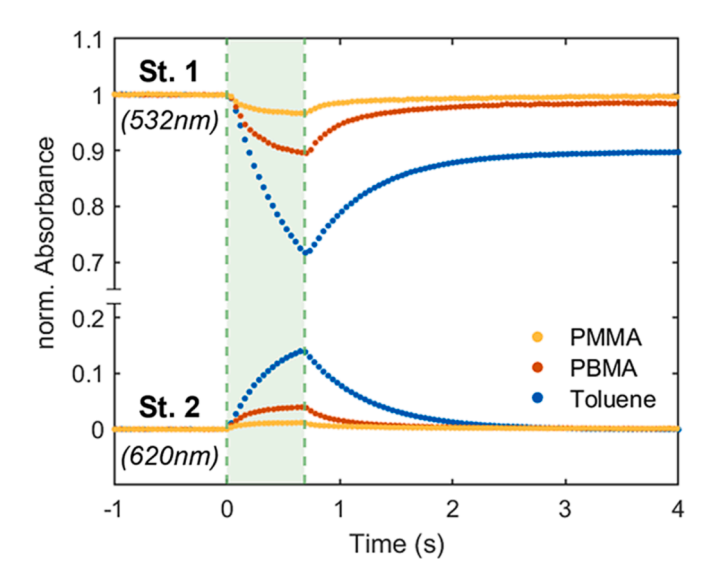


**Fig. 4.** Comparing photoisomerization rates in toluene (blue), PBMA (red), and PMMA (orange) during 600 ms of pumping with 24 mW/cm² of 532 nm light. Exposure time highlighted in green. The top three traces correspond to the *stage 1* absorbances (532 nm), while the bottom three correspond to *stage 2* (620 nm). For visualization, all three data sets were normalized to their initial *stage 1* absorbances. Normalization constants are provided in Supplementary Table S.3.

irradiation (Fig. 3C), suggested a positive correlation between the amount of *stage 2* accumulated during photoswitching and the capacity for three state kinetic control. The sample of DASA in toluene accumulated the greatest population of *stage 2* under irradiation and, as a result, displayed the greatest capacity for three state reactivity. In contrast, DASA in PBMA accumulated *stage 2* to a lesser extent and showed only slight three-state reactivity. In PMMA, DASA behaved as a purely binary switch, presumably because the *stage 2* population present during switching was too low to appreciably deplete photochemically without increasing the optical flux.

## 3.3. Quantification of thermal and photochemically accelerated stage 2 decay rates

The relationship between the pseudo-equilibrium population of *stage* 2 and the capacity for dual wavelength, multistate control was identified previously by Stricker and coworkers for two different DASA structures in solution [26]. They attributed the diminished capacity for three state reactivity in some DASAs to their comparatively shorter *stage* 2 thermal lifetimes. By this reasoning, destabilization of *stage* 2 resulted in lower *stage* 2 concentrations sustained during photobleaching and made this species largely inaccessible photochemically. However, this observation seems an unlikely explanation for the poorer kinetic control of DASA in PBMA and PMMA compared to toluene because it implies that the decay of *stage* 2 was accelerated in polymeric hosts, despite the relative lack of mobility in solids. More likely, the pseudo-equilibrium concentration of *stage* 2 was limited in polymeric hosts by lower quantum efficiencies in the isomerization of A to B, slowing the rate of *stage* 2 formation.

To support this hypothesis, we employed FMPPS to quantify the thermal decay rates of  $stage\ 2$  in PBMA, PMMA, and toluene. In this experiment, we populated  $stage\ 2$  with a brief pulse of 532 nm light and observed its subsequent decay. As further evidence for the presence of a photochemical pathway to regenerate A from B, we introduced varying intensities of 620 nm pump light during decay and determined the extent of decay rate enhancement under irradiation of  $stage\ 2$ . The proposed integrated rate law for the decay of  $stage\ 2$  is given by Eq. (1), where the effective rate constant ( $k_{eff}$ ) is given as a combination of the forward ( $k_2$ ) and reverse  $stage\ 2$  isomerization rate constants. The reverse isomerization rate constant is further broken down into thermal

 $(k_{.1})$  and photochemical components, where  $q_{620nm}$ ,  $\Phi$ , and  $\varepsilon_{St.2}$  denote the flux of the *stage 2* photoexcitation source, the reaction quantum efficiency, and the molar absorptivity of *stage 2* towards the 620 nm pump light, respectively. The absorbance as a function of elapsed time, t, after the end of the 532 nm pump pulse is given as  $A_{st.2}(t)$ . This kinetic model was exclusively valid in the low absorbance limit of *stage 2* ( $A_{St.2} < 0.043$ ) and is derived in detail in Supplementary Section S.1.

$$\ln[A_{st,2}(t)/A_{st,2}(t=0)] = -k_{eff}t \tag{1}$$

$$k_{eff} = \epsilon_{St.2} q_{620nm} \Phi_{-1} + k_{-1} + k_2 \tag{2}$$

Thermal and photochemically accelerated *stage 2* decay curves are provided in Fig. 5 for DASA in toluene, PBMA, and PMMA. All host media were observed to support a photochemical pathway to reform *stage 1*, indicated by accelerated *stage 2* decay with increasing fluxes of 620 nm light. However, this technique neglected to consider the effects of reflectance and scattering, making it challenging to extract and compare isomerization quantum yields in each medium.

Effective decay rate constants were extracted from the *stage 2* linearized decay curves (Fig. 5, bottom) by least squares regression and are presented as a function of the 620 nm pump power during decay in Fig. 6. For curves that deviated from linearity, specifically the thermally dominated decay plots in PBMA and PMMA, the effective rate constants were determined from a linear fit applied in the short time, linear regime. One possible explanation for the apparent nonlinearities in PBMA and PMMA could be the stabilization of thermal pathway to generate additional DASA isomers not accounted for in the model, including those reported by Zulfikri et al. [28]. These isomers would

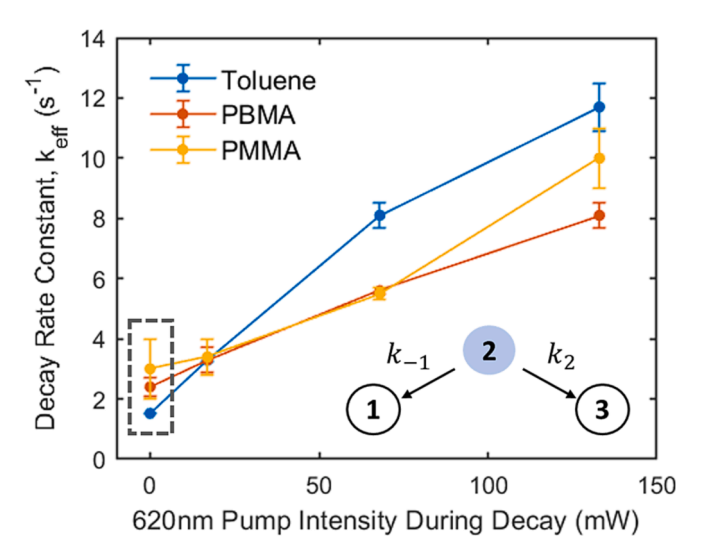


**Fig. 6.** *Stage 2* decay rate constants (see Eq. (2)) vs. incident pump power. The inset schematic illustrates the two competing decay pathways for metastable isomers in *stage 2*. Strictly thermal decay rate constants are indicated with a gray dashed box. The 620 nm pump exposure area was approx. 1.7 cm<sup>2</sup>. A full derivation of the kinetic model is provided in Supplementary Section S.1.

have been spectroscopically indistinguishable from *stages 1* and 2, making this hypothesis impossible to prove by visible absorbance measurements alone. Alternatively, the low intensity 532 nm probe light

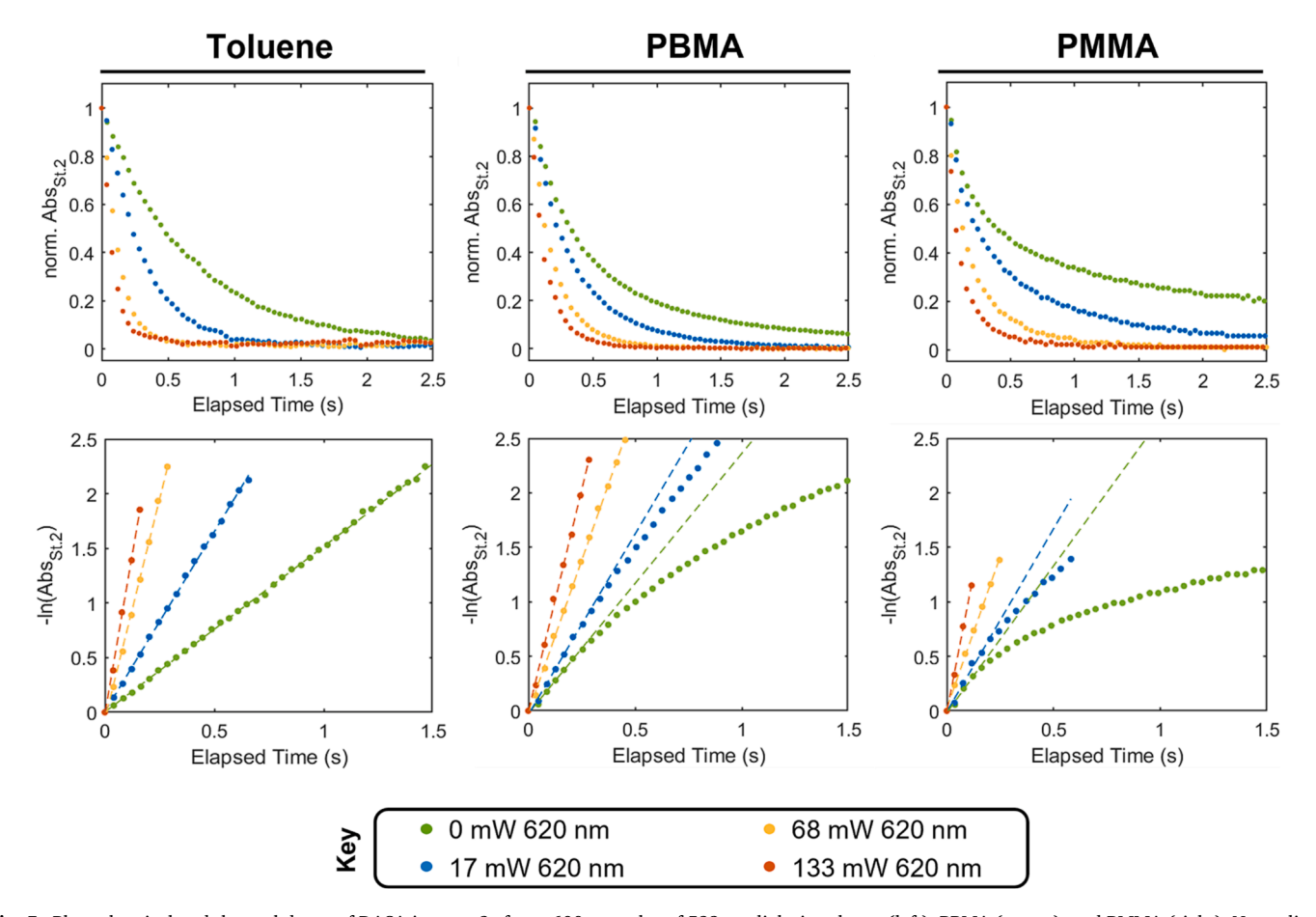


**Fig. 5.** Photochemical and thermal decay of DASA in *stage 2* after a 600 ms pulse of 532 nm light in toluene (left), PBMA (center), and PMMA (right). Normalized absorbance of the 620 nm probe source used as an indicator of *stage 2* absorbance (top). Linearization of the normalized absorbance (bottom) was used to extract a rate constant for the monoexponential decay of *stage 2* as a function of 620 nm pump intensity during decay (see key). The 620 nm pump exposure area was constant at approximately 1.7 cm<sup>2</sup>.

used to track the *stage 1* population during decay could also have introduced a small photochemical generation term not accounted for in Eq. (1). Diffusion may have limited effect of this term in toluene, where dilute species generated by the probe light could migrate out of the active probing area.

Comparing the extracted decay rate constants, we found that the strictly thermal decay rates (boxed in Fig. 6) were surprisingly similar in toluene, PBMA, and PMMA (1.52  $\pm$  0.02 s $^{-1}$ , 2.4  $\pm$  0.3 s $^{-1}$ , and 3  $\pm$  1 s $^{-1}$ , respectively). This result supported our initial hypothesis that the lower pseudo-equilibrium stage 2 populations in PBMA and PMMA were the result of slower A to B conversion, rather than accelerated thermal decay. While it seems likely that this reduction in quantum efficiency was the result of viscous forces opposing bond rotation in the polymer systems, specifically in glassy PMMA, the different molecular structures of toluene, PBMA, and PMMA make it challenging to disentangle mechanical factors from the effects of polarity.

In addition to slowing the actinic rate of *stage 2* formation, polymeric hosts were found to prevent thermal regeneration of *stage 2* from *stage 3* after complete or partial photobleaching (Supplementary Figs. S.11 & S.12). In contrast, DASA in toluene recovered to approximately 70% of its initial absorbance after 1 h in the dark following near complete conversion to *stage 3* (Supplementary Fig. S.10). This behavior has been widely reported for first generation DASA derivatives and may have further limited the degree of photokinetic control possible in PBMA and PMMA by ensuring that the formation of *stage 3* was an irreversible process.

#### 4. Conclusion

Three state photokinetic control of DASA is inhibited in systems that do not favor the accumulation of the intermediate **B** and **B**' species that make up *stage 2*. This results from the high photon fluxes required to photochemically address these dilute species. We found this phenomenon to be directly responsible for the limited and negligible degrees of photokinetic control achievable in PBMA and PMMA, respectively, compared to a solution of DASA in toluene.

To determine the cause of the limited accumulation of *stage 2* in these systems, we developed and implemented a dynamic, phase-locked spectroscopic technique (FMPPS) with higher sampling speeds and greater sensitivity than standard UV–Vis to probe the photochemical evolution and rapid decay of *stage 2*. With FMPPS, we found that transitioning from a toluene solution to polymeric hosts resulted in the emergence of nonlinear *stage 2* thermal decay kinetics, but minimal change in the thermal stability of this stage, as reflected in its initial decay rate following the cessation of *stage 1* excitation. This suggested that the reduction in *stage 2* accumulation in PBMA and PMMA compared to toluene resulted primarily from slower actinic A to B conversion and could likely be attributed to viscous effects, which have been reported previously to influence DASA switching kinetics in polymers [1,32].

One additional factor which may have contributed to the limited accumulation of stage 2 in PBMA and PMMA was the lack of a thermally accessible pathway to regenerate B' from C during photobleaching. Thermal open form recovery, which occurred slower relative to the preceding isomerizations in toluene, likely provided a small boost in the pseudo-equilibrium stage 2 population established during bleaching in toluene but not in the polymeric hosts. While this study did not consider the possibility of a photochemical pathway in the isomerization of **B**' to C, as was suggested by Bieske and coworkers for DASA in the gas phase, this may have also contributed slightly to efficacy of dual wavelength photokinetic control by simultaneously accelerating both competing  $stage\ 2$  decay pathways with the same wavelength of light [35]. If this effect could primarily account for the reduced photokinetic control in PBMA and PMMA, we would expect the photochemical stage 2 decay rates constants in Fig. 6 to increase faster with the intensity of 620 nm light in PBMA and PMMA. However, this was not observed.

While this study succeeds in identifying crucial steps in the overall DASA photobleaching process that result in the observed matrix effects limiting the three-state reactivity in PBMA and PMMA, the underlying reasons for these effects require further study. To that end, additional work is necessary before one can implement a systematic approach to structurally modifying the DASA architectures or host polymers with the objective of offsetting these kinetic matrix effects and enabling dynamic, three state photoswitching in polymeric hosts.

#### CRediT authorship contribution statement

Sara Sandlass: Writing – review & editing, Writing – original draft, Visualization, Methodology, Investigation, Formal analysis, Data curation, Conceptualization. Friedrich Stricker: Resources, Conceptualization. Daniel Fragoso: Investigation. Javier Read de Alaniz: Writing – review & editing, Supervision, Funding acquisition, Conceptualization. Michael J. Gordon: Writing – review & editing, Supervision, Project administration, Methodology, Funding acquisition, Conceptualization.

#### **Declaration of Competing Interest**

The authors declare that they have no known competing financial interests or personal relationships that could have appeared to influence the work reported in this paper.

#### Data availability

Data will be made available on request.

#### Acknowledgements

This work was supported by the NSF EFRI program under grant no. 1935327, and leveraged equipment supported by an NSF Career award, grant no. 0953441. The authors acknowledge the use of the MRL Shared Experimental Facilities supported by the MRSEC Program of the NSF under award no. DMR 1720256, a member of the NSF-funded Materials Research Facilities Network (www.mrfn.org).

#### **Author Contributions**

This work was conceptualized by S.S., M.J.G., F.S., and J.RdA. Method development by S.S. and M.J.G. Experiments conducted by S.S and D.F. Project was supervised by M.J.G. and J.RdA. DASA synthesis by F.S. S.S composed the manuscript with guidance and edits from J.RdA and M.J.G.

#### Appendix A. Supplementary data

Supplementary data (Contains a derivation of the kinetic model and additional spectroscopic data. Tables S.1-S.3, Figures S.1-S.12.) to this article can be found online at https://doi.org/10.1016/j.jphotochem.20 23 114964

#### References

- [1] S. Ulrich, J.R. Hemmer, Z.A. Page, N.D. Dolinski, O. Rifaie-Graham, N. Bruns, C. J. Hawker, L.F. Boesel, J. Read De Alaniz, Visible light-responsive DASA-polymer conjugates, ACS Macro Lett. 6 (7) (2017) 738–742, https://doi.org/10.1021/acsmacrolett/7b00350
- [2] L. Mao, Z. Wang, Y. Duan, C. Xiong, C. He, X. Deng, Y. Zheng, D. Wang, Designing of rewritable paper by hydrochromic donor-acceptor stenhouse adducts, ACS Nano 15 (6) (2021) 10384–10392. https://doi.org/10.1021/acsnano.1c02629.
- [3] G. Szalöki, G. Sevez, J. Berthet, J.L. Pozzo, S. Delbaere, A simple molecule-based octastate switch, J. Am. Chem. Soc. 136 (39) (2014) 13510–13513, https://doi. org/10.1021/ja506320j.
- [4] W. Francis, A. Dunne, C. Delaney, L. Florea, D. Diamond, Spiropyran based hydrogels actuators—Walking in the light, Sens. Actuators B Chem. 250 (2017) 608–616, https://doi.org/10.1016/j.snb.2017.05.005.

- [5] C. Li, A. Iscen, L.C. Palmer, G.C. Schatz, S.I. Stupp, Light-driven expansion of spiropyran hydrogels, J. Am. Chem. Soc. 142 (18) (2020) 8447–8453, https://doi. org/10.1021/jacs.0c02201.
- [6] R.F. Khairutdinov, J.K. Hurst, Photocontrol of ion permeation through bilayer membranes using an amphiphilic spiropyran, Langmuir 17 (22) (2001) 6881–6886, https://doi.org/10.1021/la010756r.
- [7] L. Zhao, S. Seshadri, X. Liang, S.J. Bailey, M. Haggmark, M. Gordon, M.E. Helgeson, J. Read de Alaniz, P. Luzzatto-Fegiz, Y. Zhu, Depinning of multiphase fluid using light and photo-responsive surfactants, ACS Cent. Sci. 8 (2) (2022) 235–245, https://doi.org/10.1021/acscentsci.1c01127.
- [8] S. Seshadri, S.J. Bailey, L. Zhao, J. Fisher, M. Sroda, M. Chiu, F. Stricker, M. T. Valentine, J. Read De Alaniz, M.E. Helgeson, Influence of polarity change and photophysical effects on photosurfactant-driven wetting, Langmuir 37 (33) (2021) 9939–9951, https://doi.org/10.1021/acs.langmuir.1c00769.
- [9] T.J. Gately, W. Li, S.H. Mostafavi, C.J. Bardeen, Reversible adhesion switching using spiropyran photoisomerization in a high glass transition temperature polymer, Macromolecules 54 (20) (2021) 9319–9326, https://doi.org/10.1021/ acs.macromol.1c01262.
- [10] X. Lu, S. Guo, X. Tong, H. Xia, Y. Zhao, Tunable photocontrolled motions using stored strain energy in malleable azobenzene liquid crystalline polymer actuators, Adv. Mater. 29 (28) (2017) 1606467, https://doi.org/10.1002/adma.201606467.
- [11] Z. Jiang, Y. Xiao, X. Tong, Y. Zhao, Selective decrosslinking in liquid crystal polymer actuators for optical reconfiguration of origami and light-fueled locomotion, Angew. Chem. 131 (16) (2019) 5386–5391, https://doi.org/10.1002/ ange.201900470
- [12] M. Lahikainen, H. Zeng, A. Priimagi, Reconfigurable photoactuator through synergistic use of photochemical and photothermal effects, Nat. Commun. 9 (1) (2018), https://doi.org/10.1038/s41467-018-06647-7.
- [13] R.C.P. Verpaalen, M. Pilz da Cunha, T.A.P. Engels, M.G. Debije, A.P.H. J. Schenning, Liquid crystal networks on thermoplastics: reprogrammable photoresponsive actuators, Angew. Chem. 132 (11) (2020) 4562–4566, https://doi.org/ 10.1002/ange.201915147.
- [14] M. Chen, B. Yao, M. Kappl, S. Liu, J. Yuan, R. Berger, F. Zhang, H.-J. Butt, Y. Liu, S. i. Wu, Entangled azobenzene-containing polymers with photoinduced reversible solid-to-liquid transitions for healable and reprocessable photoactuators, Adv. Funct. Mater. 30 (4) (2020) 1906752, https://doi.org/10.1002/adfm.201906752.
- [15] S. Helmy, F.A. Leibfarth, S. Oh, J.E. Poelma, C.J. Hawker, J.R. De Alaniz, Photoswitching using visible light: A new class of organic photochromic molecules, J. Am. Chem. Soc. 136 (23) (2014) 8169–8172, https://doi.org/10.1021/ ia503016b.
- [16] M.M. Sroda, J. Lee, Y. Kwon, F. Stricker, M. Park, M.T. Valentine, J. Read de Alaniz, Role of material composition in photothermal actuation of DASA-based polymers, ACS Appl Polym Mater 4 (1) (2022) 141–149, https://doi.org/10.1021/ acsapm.1c01108.
- [17] J. Lee, M.M. Sroda, Y. Kwon, S. El-Arid, S. Seshadri, L.F. Gockowski, E.W. Hawkes, M.T. Valentine, J. Read De Alaniz, Tunable photothermal actuation enabled by photoswitching of donor-acceptor stenhouse adducts, ACS Appl. Mater. Interfaces 12 (48) (2020) 54075–54082, https://doi.org/10.1021/acsami.0c15116.
- [18] S. Seshadri, L.F. Gockowski, J. Lee, M. Sroda, M.E. Helgeson, J. Read de Alaniz, M. T. Valentine, Self-regulating photochemical Rayleigh-Bénard convection using a highly-absorbing organic photoswitch, Nat. Commun. 11 (1) (2020), https://doi.org/10.1038/s41467-020-16277-7.
- [19] O. Rifaie-Graham, S. Ulrich, N.F.B. Galensowske, S. Balog, M. Chami, D. Rentsch, J. R. Hemmer, J. Read De Alaniz, L.F. Boesel, N. Bruns, Wavelength-selective light-responsive DASA-functionalized polymersome nanoreactors, J. Am. Chem. Soc. 140 (25) (2018) 8027–8036, https://doi.org/10.1021/jacs.8b04511.
- [20] S. Jia, A. Tan, A. Hawley, B. Graham, B.J. Boyd, Visible light-triggered cargo release from Donor Acceptor Stenhouse Adduct (DASA)-doped lyotropic liquid

- crystalline nanoparticles, J. Colloid Interface Sci. 548 (2019) 151–159, https://doi.org/10.1016/j.jcis.2019.04.032.
- [21] S. Jia, J.D. Du, A. Hawley, W.K. Fong, B. Graham, B.J. Boyd, Investigation of donor-acceptor Stenhouse adducts as new visible wavelength-responsive switching elements for lipid-based liquid crystalline systems, Langmuir 33 (9) (2017) 2215–2221, https://doi.org/10.1021/acs.langmuir.6b03726.
- [22] W. Hou, R. Liu, S. Bi, Q. He, H. Wang, J. Gu, Photo-responsive polymersomes as drug delivery system for potential medical applications, Molecules 25 (21) (2020) 542–552, https://doi.org/10.3390/molecules25215147.
- [23] Y.J. Diaz, Z.A. Page, A.S. Knight, N.J. Treat, J.R. Hemmer, C.J. Hawker, J. Read de Alaniz, A versatile and highly selective colorimetric sensor for the detection of amines, Chem. A Eur. J. 23 (15) (2017) 3562–3566, https://doi.org/10.1002/ chem. 201700368
- [24] B.P. Mason, M. Whittaker, J. Hemmer, S. Arora, A. Harper, S. Alnemrat, A. McEachen, S. Helmy, J. Read De Alaniz, J.P. Hooper, A temperature-mapping molecular sensor for polyurethane-based elastomers. *Appl. Phys. Lett.* 108 (4) (2016). 10.1063/1.4940750.
- [25] H. Zhao, X. Qin, L. Zhao, S. Dong, L. Gu, W. Sun, D. Wang, Y. Zheng, Invisible inks for secrecy and anticounterfeiting: from single to double-encryption by hydrochromic molecules, ACS Appl. Mater. Interfaces 12 (7) (2020) 8952–8960, https://doi.org/10.1021/acsami.0c00462.
- [26] F. Stricker, D.M. Sanchez, U. Raucci, N.D. Dolinski, M.S. Zayas, J. Meisner, C. J. Hawker, T.J. Martínez, J. Read de Alaniz, A multi-stage single photochrome system for controlled photoswitching responses, Nat. Chem. 14 (8) (2022) 942–948, https://doi.org/10.1038/s41557-022-00947-8.
- [27] M. Di Donato, M.M. Lerch, A. Lapini, A.D. Laurent, A. Iagatti, L. Bussotti, S.P. Ihrig, M. Medved, D. Jacquemin, W. Szymański, W.J. Buma, P. Foggi, B.L. Feringa, Shedding light on the photoisomerization pathway of donor-acceptor stenhouse adducts, J. Am. Chem. Soc. 139 (44) (2017) 15596–15599, https://doi.org/10.1021/jacs.7b09081.
- [28] H. Zulfikri, M.A.J. Koenis, M.M. Lerch, M. Di Donato, W. Szymański, C. Filippi, B. L. Feringa, W.J. Buma, Taming the complexity of donor-acceptor Stenhouse adducts: infrared motion pictures of the complete switching pathway, J. Am. Chem. Soc. 141 (18) (2019) 7376–7384, https://doi.org/10.1021/jacs.9b00341.
- [29] R. Davis, N. Tamaoki, Modulation of unconventional fluorescence of novel photochromic perimidine spirodimers, Chem. A Eur. J. 13 (2) (2007) 626–631, https://doi.org/10.1002/chem.200600190.
- [30] M.M. Sroda, F. Stricker, J.A. Peterson, A. Bernal, J. Read de Alaniz, Donor-acceptor Stenhouse adducts: exploring the effects of ionic character, Chem. A Eur. J. 27 (12) (2021) 4183–4190, https://doi.org/10.1002/chem.202005110.
- [31] M.M. Lerch, M. Di Donato, A.D. Laurent, M. Medved', A. Iagatti, L. Bussotti, A. Lapini, W.J. Buma, P. Foggi, W. Szymański, B.L. Feringa, Solvent effects on the actinic step of donor-acceptor Stenhouse adduct photoswitching, Angew. Chem. 130 (27) (2018) 8195–8200.
- [32] R. McDonough, N. Rudgley, O. Majewski, M.V. Perkins, R.A. Evans, D.A. Lewis, Photochromic performance of donor-acceptor stenhouse adducts in polymer binders and solution, ChemPhotoChem 6 (9) (2022), https://doi.org/10.1002/ cptc 202200076
- [33] B.F. Lui, N.T. Tierce, F. Tong, M.M. Sroda, H. Lu, J.R. de Alani, C.J. Bardeen, Unusual concentration dependence of the photoisomerization reaction in donoracceptor Stenhouse adducts, Photochem. Photobiol. Sci. 18 (6) (2019) 1587–1595.
- [34] M.M. Lerch, S.J. Wezenberg, W. Szymanski, B.L. Feringa, Unraveling the photoswitching mechanism in donor-acceptor Stenhouse adducts, J. Am. Chem. Soc. 138 (20) (2016) 6344–6347, https://doi.org/10.1021/jacs.6b01722.
- [35] J.N. Bull, E. Carrascosa, N. Mallo, M.S. Scholz, G. Da Silva, J.E. Beves, E.J. Bieske, Photoswitching an isolated donor-acceptor Stenhouse adduct, J. Phys. Chem. Lett. 9 (3) (2018) 665–671, https://doi.org/10.1021/acs.jpclett.7b03402.